FCC-ee Detector Studies

Performance study for different geometries of the future Noble Liquid calorimeter at FCC-ee
September 3, 2021

CERN summer student report

Abstract:
This document summarizes detector performance studies carried out for different versions of the Noble Liquid electromagnetic calorimeter proposed for FCC-ee. The energy and angular resolutions are presented for various combinations of absorber material, Noble Liquid and sensitive gap thickness. In addition to this, the effect of the cell merging strategy at the read-out level is also evaluated.

Mark Waterlaat
mail: markwaterlaat@gmail.com
Supervisors: Dr. Brieuc Francois
Dr. Martin Aleksa

Part 1

Overview

The FCC-ee is a future lepton collider operated in a 100 km circular tunnel in the Geneva area[1]. The FCC-ee is brought into life as the first phase of the *Future Circular Collider* (FCC) integrated program, the current proposal for a post-LHC flagship experiment. The FCC-ee will fucntion as a frontier Higgs, Top, Electroweak and flavour factory and has to be equipped with outstanding detector technologies in order to meet it's very demanding physics program[2]. To perform these measurements a high granularity, very good energy resolution and strong control over the systematic uncertainties and acceptance all together is needed.

Noble Liquid based calorimetry is a promising candidate to fulfil these requirements and thus there is a strong R&D effort ongoing to design a new generation Noble Liquid calorimeter. Current design for the FCC-ee has multiple interaction points where detectors are to be placed. The option for a Noble Liquid calorimeter is currently studied as part of the IDEA detector design [3]. The calorimeter will be a sampling type calorimeter consisting of inclined passive absorber plates along with the active Noble Liquid all at cryogenic temperatures. A schematic overview of the current Noble Liquid calorimeter being studied can be seen in figure 1.

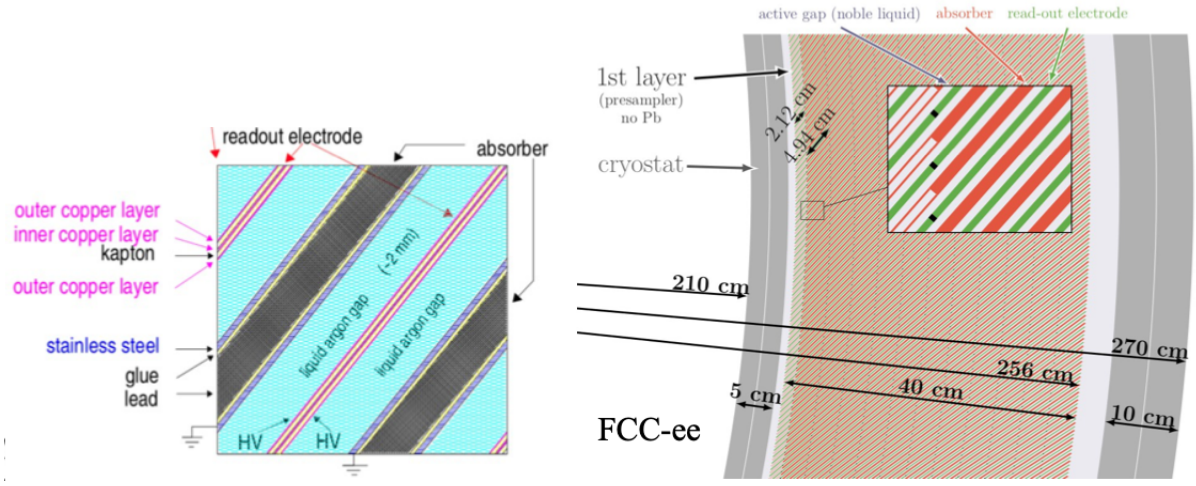

Figure 1: (left)Schematic view of the different volumes present in a physical cell in the similar ATLAS EMCal. While the FCC does not make use of the accordion geometry, the stacked volumes are similar. (right) Schematic radial cross section of the calorimeter with PCB's in green, passive plates in red.

This report aims to see the impact on performance in both energy resolution as well as angular resolution of different geometries. The geometries are tweaked in a way that the calorimeter including the needed cryostat and service volume account for 22 (radiation lengths) X_0.

Part 2

Simulation Setup

2.1 Software

To study the performance of different geometry designs, simulations have to be done using the FCC software. This consists of the FCCAnalyses, FCCDetectors, k4FWCore, k4RecCalorimeter, k4SimGeant4 repositories [4]. These repositories have been downloaded and compiled locally on lxplus where modifications are made. To generate new data a couple of steps have to be taken in order. These are:

- Change the geometry definition
- Determine sampling fraction
- Determine dead material correction
- Do the full calorimeter reconstruction

After these steps, the data can be analysed and used to determine the performance. These steps then have to be repeated for all geometries separately.

All simulations presented in this report are done using a GEANT4 particle gun aimed centrally in the detector. This combined with the lack of noise or detector non-uniformities will mean presented results will show a best case scenario.

For the sampling fraction simulations the volume placed in the mother volume will be the EMCal, service volume and cryostat. The simulations then store both the energy in the Noble Liquid as well as the entire detector. The ratio of these two can then later be filled in a histogram and fitted with a gaussian to determine the peak position. This process will then be repeated for all layers in the calorimeter to get the final correction factors. Because Noble Liquid calorimeters have been proven to have great linearity, this is only done in for 1 energy point[5].

After the sampling fraction is known the dead material corrections have to be determined. This correction is introduced to compensate for missing signal in the caloriemeter. This includes energy deposit in the passive cryostat around the calorimeter as well as leakage outside the calorimeter all together. This correction is done by correlating the energy deposit in the layer closest to the dead material in question. This will be the first layer with the front cryostat for the upstream correction and the last with the cryostat back wall for the downstream correction. The relation between the energy deposit in the first/last layer and corresponding dead material is energy dependant, and thus the corrections need to be as well.

Which function is used to describe the dependancy of the missing signal in the calorimeter is user defined. These functions however need to be fitted to energy dependant parameters themselves. This implies a first fit on a set energy is needed after which an energy dependant parameter fit can be done.

The function used for the upstream corrections in this report is always a 1st order polynomial. This in contrast to the downstream corrections which uses 2nd order polynomials. After all energies have their polynomials fitted, the energy dependance of the coefficients can be determined. This is done by fitting yet another user defined function to the data which gives the final corrections. These functions with their fitted parameters are then used as an input for the final calorimeter reconstruction.

The final simulation step is to do the full detector reconstruction. This is done by adding the other sub-detectors volumes in the simulation, to get a realistic material budget, although the information they provide is not used in this study. The simulations done for the full reconstruction store the energy deposited in each sensitive cell. Afterwards this information is processed to form clusters using a sliding window algorithm. The clusters, in contrary to cell hits, will contain angular info which is needed for the performance studies. It is important to note here that the cluster data is corrected for dead material, where as the cell data is not. The cell information is however still stored for comparison.

2.2 Geometry

Using the steps described in section 2.1, different geometries can be studied. The baseline geometry used in simulations is a Noble Liquid calorimeter with lead absorbers and *Liquid Argon* (LAr) as an active medium. For structural support the lead absorbers are glued to a steel plate using G10 resin. The signal is collected using a PCB placed in the middle of the Noble Liquid gap in between passive plates. Because of this a physical cell is defined as a stack of: ($\frac{1}{2}$Passive plate + Liquid gap + PCB + Liquid gap + $\frac{1}{2}$Passive plate). A high voltage is then applied to the PCB plate while connecting the absorbers to ground. This provides a voltage difference collecting the signal from the Noble Liquid.

These physical cells are then layered along a radius inside the cryostat[1]. The baseline geometry is tuned to have 1536 passive plates and PCBs under a 50 degree inclination. This number of passive

[1] This radius is shifted a bit from the cryostat wall to have a small service volume

planes is in turn also the origin of the calorimeters ϕ segmentation. Looking deeper into figure 1(right), numbers for the inner cryostat volumes as well as the starting radius for the calorimeter can be seen. These numbers, as well as the PCB thickness, will be constant in all setups. The rest of the dimensions will be tuned to each specific scenario. Changes include the thickness of the Noble Liquid gap, Noble Liquid choice, absorber material for sampling calorimeters.

When taking a deeper look into the shape of each physical cell, it can be noted that the Noble Liquid gap has a trapezoidal shape. This is because the circumference growing with the radius of the calorimeter while the passive planes remain equal in thickness. To make sure all scenarios are compared the right way, only the gap size at the start of the calorimeter is defined. The code will then propagate the gap size growth itself without needing further input.

Going back to the baseline scenario and looking into the read-out side of things, some feautres have to be noted as well. To limit the number of read-out channels that need to pass from the cryogenic to the ambient side of the cryostat, 2 physical cells are merged into 1 read-out cell. In simulations this is done by simply adding the signal of the two relevant cells and treating them as one. However studies have also been carried out on the impact on performance of a different number. This would be merging 1,2,3,4,6physical cells and see what impact this has. Parallel to the merger at read-out level, the effect of having a twice bigger physical cell[2] has also been explored. This doubling of the physical cell would alleviate the need of merging cells on read-out level[3].

Besides the sampling calorimeters the performance of a homogeneous Noble Liquid calorimeter has also been studied. This has been done in the software by setting the thickness in the passive plates from a total of 2 mm to a new total of 0.003 mm. Apart from changing the dimensions of the passive plates, the material is also set to the same Noble Liquid as present in the active gaps. Important to note here is the fact that the PCB's remain unchanged compared to the baseline setup. Due to the relatively large $X_0$from LAr, only LKr and LXe have been considered for these geometries since the radial extend would be too much over the 40 cm baseline.

As well as being segmented in ϕ, the calorimeter is also segmented in θ as well as radially. The θ segmentation is kept constant during all geometries and is defined as an angular range from $45° \leq \theta \leq 135°$ with a interval of $\Delta\eta = 0.01$[4].

Radially the calorimeter is segmented in 12 total layers. In the case of the sampling calorimeters layer 0 is a shorter pre-sampler layer without a dense layer in the passive planes. The other 11 layers are defined as equal in length with the passive plates as previously stated. The length of these radial segments is calculated by defining an approximately 1.5 cm pre-sampler and dividing the remaining radial extend needed in 11 parts. For the homogeneous setups, all 12 layers are defined equally as the radial extend divided by 12.

Looking in table 1, an overview of all important design parameters is geven. To be able to compare similar geometries with different radial extends, the sensitive gap size for the W + LAr geometry has been tuned to have a similar sampling fraction to the baseline Pb + LAr. This is done by changing the number of passive plates with an increment of 64[5] and calculating the gap size needed for this.

Table 1: Geometry definitions

Absorber	Liquid	Gap size [mm]	Absorber size [mm]	Physical cells	Read-out cells	Radial extent [mm]
Pb	LAr	$1.239 \cdot 2$	1.8	1536	1536, 768, 512, 384, 256	400
	LAr	$3.079 \cdot 2$	3.8	768	768	400
	LKr	$1.239 \cdot 2$	1.8	1536	768	400
W	LAr	$2.156 \cdot 2$	1.8	1536	768	≈ 323.9
	LKr	$1.239 \cdot 2$	1.8	1536	768	≈ 207.5
none	LKr	≈ 4.2	0.001	1536	768	≈ 1034
	LXe	≈ 4.2	0.001	1536	768	≈ 647.5

[2]This means the steel, glue as well as the PCB' size are kept constant

[3]This geometry setup will later be referred to as "Double"

[4]The step being in η originates from the FCC-hh design being a hadronic collider

[5]This is for final production purposes

Part 3
Results

In this section the analysed data will be given and discussed for all geometries.

3.1 Sampling fraction

The first step in obtaining the detector performance is getting the sampling fraction. This is done by simulating 10k 45 GeV photon events from the particle gun. Figure 2 shows some of the distributions used for fitting the sampling fractions.

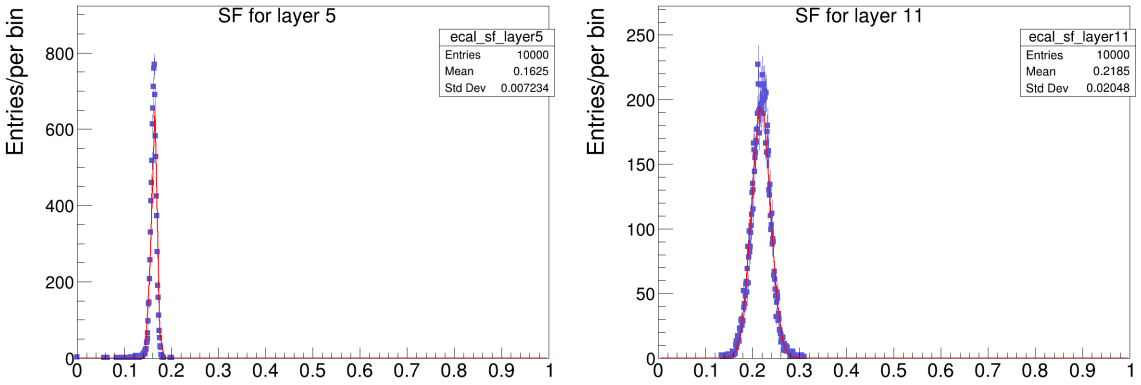

Figure 2: Distributions of measured sampling fractions for baseline Pb + LAr geometry in layer 5 (left) and layer 11(right)

As said the sampling fraction needs to be determined for each layer in a given geometry. When comparing different geometries these peak positions can be plotted and compared to each other as can be seen in figure 3.

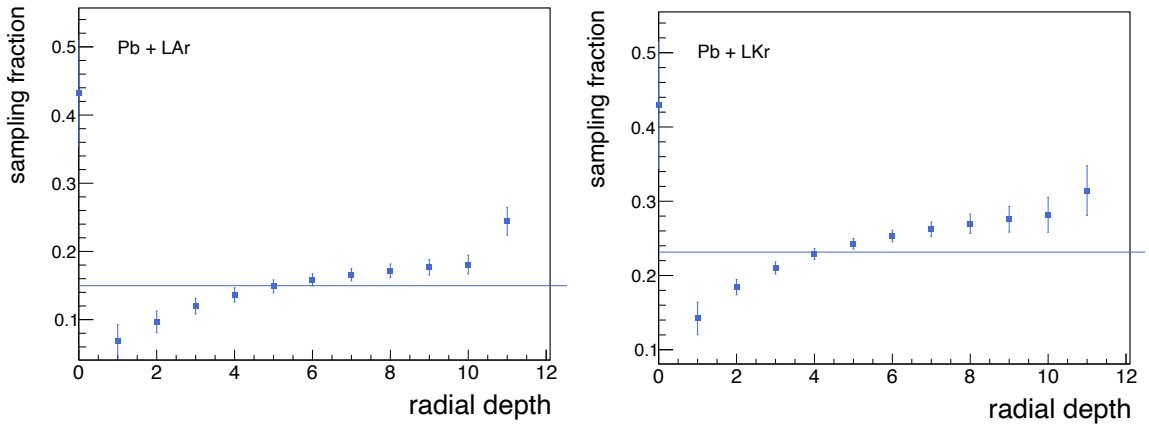

Figure 3: Sampling fraction as a function of layer number for baseline Pb + LAr (left) and Pb + LKr with the same dimensions (right)

As can be seen in figure 3 the average sampling fraction in the Pb + LKr setup[6] is higher compared

[6]This is also the only geometry with more than 22 X_0. Only 337.5 mm radially would be needed in the case of a Pb + LKr

to the baseline Pb + LAr. This is as expected since the only difference in setups is the choice of Noble Liquid. Since the radiation length of LKr is about 3 times higher compared to LAr, more signal in the active volume is expected. As can be seen in both plots shown, there is a relatively high sampling fraction in layer 0. This is due to the lack of dense material in the pre-sampler. The steady increase from layer 1-11 can be explained by the growing Noble Liquid gap size in the radial direction.

Looking at all the different geometries, the average sampling fractions can be found in table 2.

Table 2: Average sampling fraction for different geometries

	Average sampling fraction
Pb + LAr (baseline)	0.17
Pb + LKr	0.23
Pb + LAr (double)	0.17
W + LKr	0.15
W + LAr	0.16
LKr (homo)	0.97
LXe (homo)	0.97

When comparing the average sampling fraction of the baseline scenario and W + LAr, it can be seen that there still is a difference present. This is due to the fact that the number of physical cells has to be a multiple of 64, thus constraining the gap size.

3.2 Dead material correction

The upstream and downstream corrections are determined separately from each other but in a similar process as described in section 2.1. Some of the different individual profiles used for the upstream correction are given in figure 4 for the baseline Pb + LAr geometry.

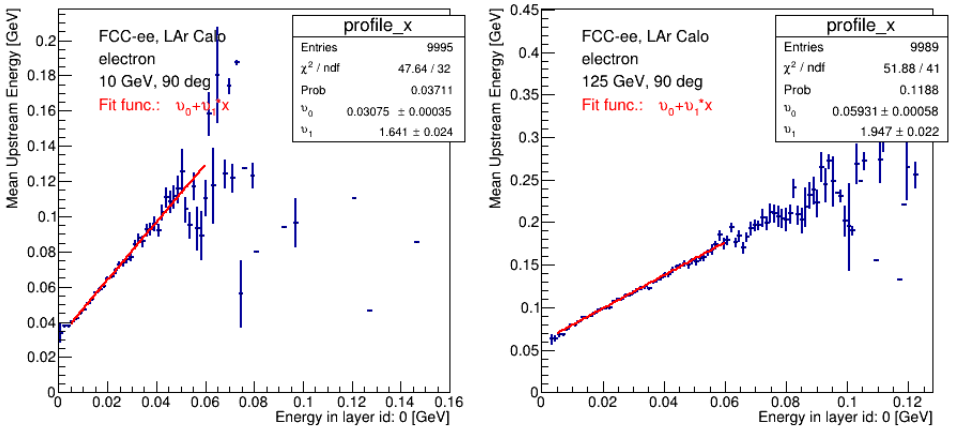

Figure 4: Fitted profiles for upstream energy correction for baseline Pb + LAr detector with 10 GeV photons (left) and 125 GeV photons (right). Plots show the energy deposited in layer 0 on the horizontal axis with the deposit in the cryostat on the vertical axis.

Looking at the points in figure 4, the lower energy deposits in layer 0 give a clear correlation, while the higher energies show more fluctuations. Due to this effect, attention has to be paid to the fitting range to avoid wrong fits. After the individual energies have been fitted, the final parameter fit can be done as shown in figure 5.

geometry.

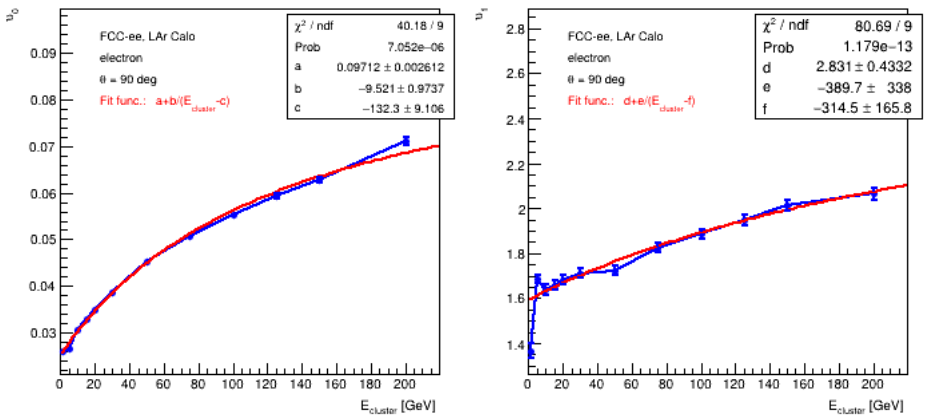

Figure 5: Parameter fit for upstream correction in baseline Pb + LAr geometry with parameter v_0 (left) and v_1 (right)

Looking first at the baseline Pb + LAr shown in figure 5, it can be seen that the graph's points have relative small errors as well as the fact that the fit describes all points pretty good.

The steps needed to obtain the downstream correction are, as said before, almost identical to the upstream correction. Some of the individual energy points for the baseline Pb + LAr are given in figure 6.

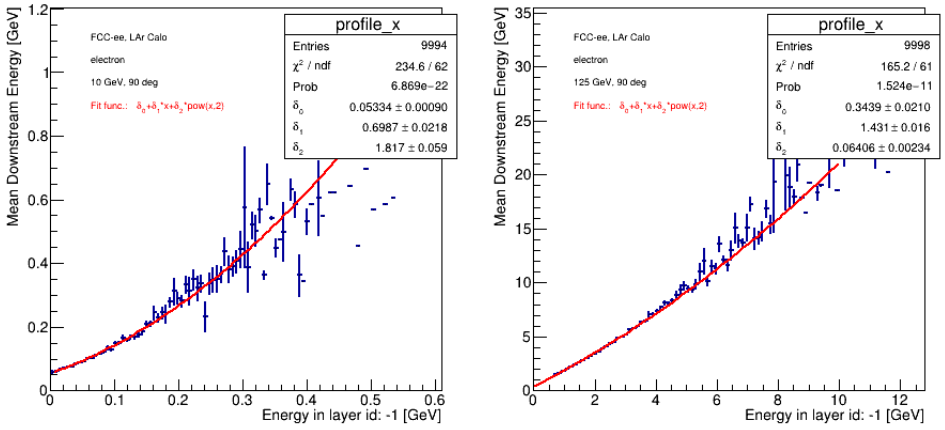

Figure 6: Fitted profiles for the downstream correction in the baseline Pb + LAr geometry for 10 GeV (left) and 125 GeV (right)

And identical to the upstream correction the final parameter fit is obtained from these plots and shown in figure 7.

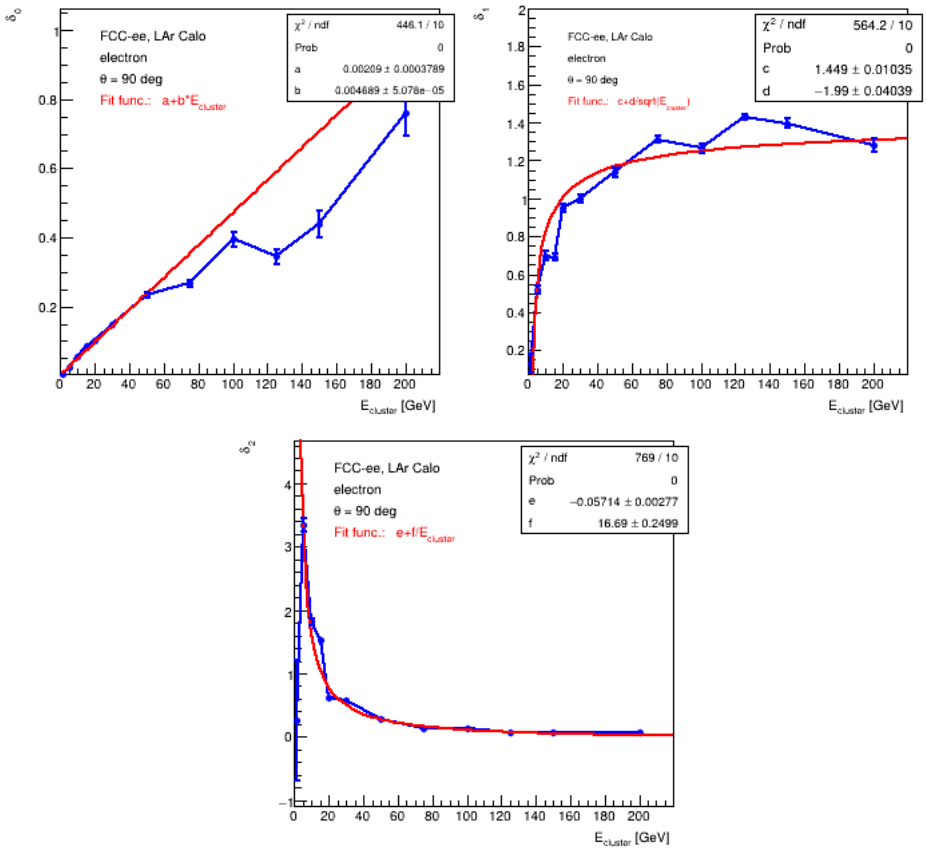

Figure 7: Parameter fit for downstream correction in the baseline Pb + LAr geometry.

After both corrections have been determined, the impact on detector responses can be studied. This is done by comparing the detector response for the corrected cluster data with the uncorrected cell data. This is shown for the baseline Pb + LAr geometry in figure 8.

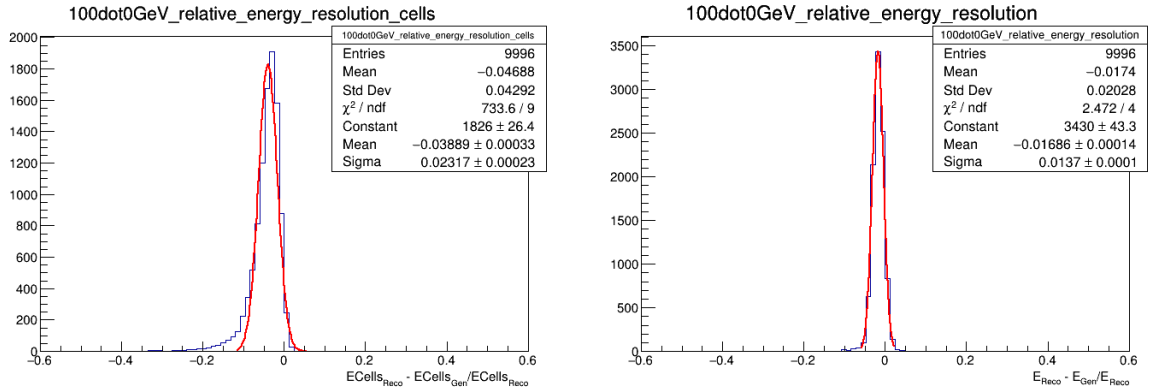

Figure 8: Detectore response for 100 GeV photons in the baseline Pb + LAr geometry. (left) Detector response for the uncorrected cells, shows a low energy tail. (right) Shows the corrected cluster detector response in which the low energy tail disappeared, improving the resolution.

The cell data shown in figure 8 is obtained by summing all energy deposits present in the full calorimeter. This is possible because the simulations are done using a particle gun, ergo all deposits are signal. The disappearing low energy tail in the cluster response shows the dead material corrections

are applied correctly and help improve the energy resolution.

3.3 Energy resolution

Implementing all previous steps, the energy resolution for each geometry is now determined. This is done by fitting the detector response for all simulated energies using both cell and cluster data. This is shown to indicate the impact of the dead material correction[7]. The energy resolution curves of different geometries are shown in figure 9, with the fitted parameters given in table B in appendix A.

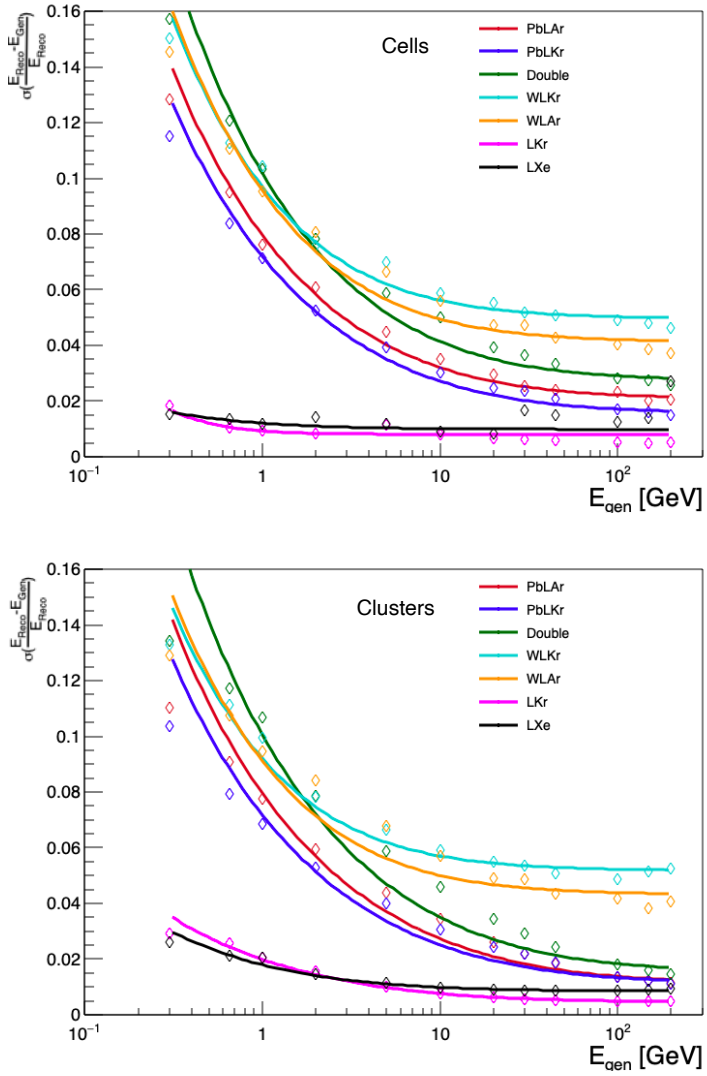

Figure 9: Energy resolution curves for different geometries using cells (top) and clusters (bottom). Important to note is the lack of downstream correction in the W + LKr and W + LAr geometries

Comparing different geometries shown in figure 9, some other features can be seen. The homogeneous calorimeters perform best as expected. The sampling fraction here is almost 1 and as of yet no noise or detector non-uniformities have been introduced.

Comparing the baseline Pb + LAr to the Pb + LKr geometry shows an expected improvement in

[7] The clustering algorithm will also impact performance a bit, but since there is only 1 generated particle this effect is small.

resolution for the Pb + LKr. This can be attributed to the higher sampling fraction of the Pb + LKr setup. However the doubled physical cell performs significantly worst compared to baseline.

When comparing the cell data with the cluster data, it can be seen that clusters perform better in general, as expected due to the applied corrections. The downstream corrections have however been removed from the W + LKr and W + LAr geometries due some unexpected behaviour. When taking a deeper look into the W + LKr geometry, studies have been done with the inclusion of the downstream corrections. Besides applying the downstream correction, the effect of halving the physical cell size has also been studied, the impact of these changes can be seen in figure 10[8].

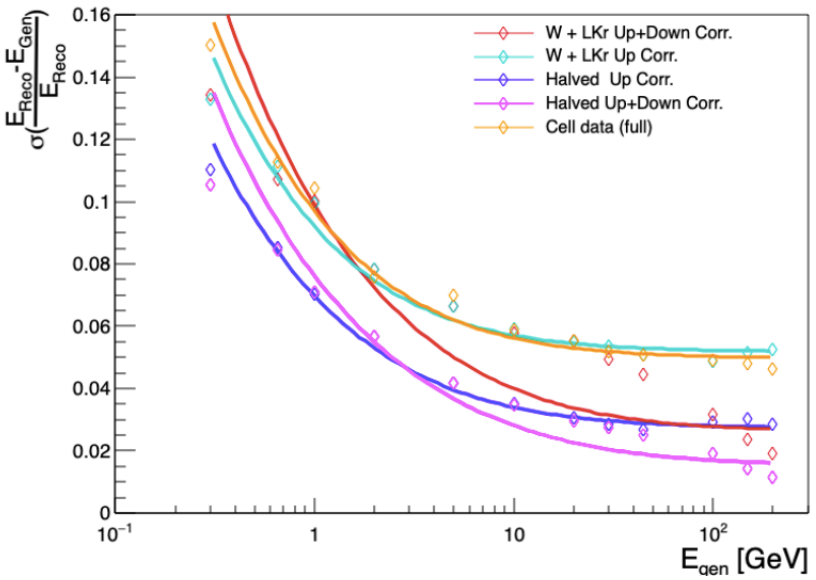

Figure 10: Comparison for the energy resolution of W + LKr different geometries as well as comparing the downstream corrected data with the downstream uncorrected data.

Looking to the different geometries used in figure 10[9] it can be seen that the shoulder forming in the downstream corrected data shows in both the nominal W + LKr and the halved cell size. This shows the effect is consistent within multiple geometries and makes a good argument for the dead material corrections to be correct. It can also be seen that the dead material corrections only improve the resolution, so while deviating from the fit, the correction improves performance.

Moving from merging cells on physical level towards merger at read-out level, the different energy resolutions are given in figure 11.

[8] Parameters can be found in appendix B. Geometry dimensions: gap size = 0.359874*2*mm, absorber size = 0.9 mm, G10 = Steel = 0.01 mm

[9] The Cell data shown is from the nominal W + LKr setup only.

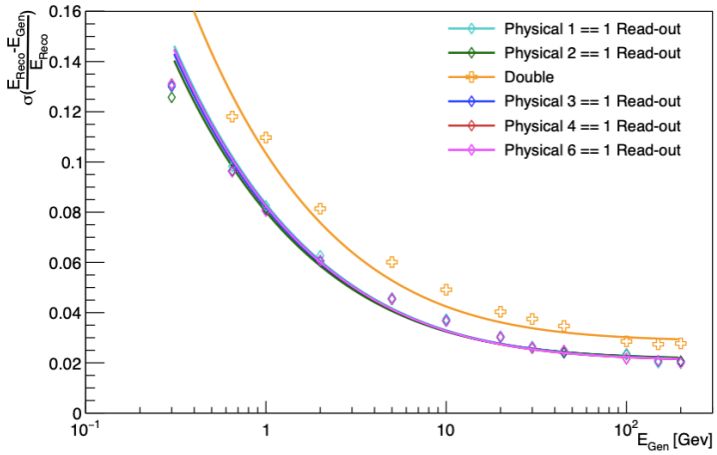

Figure 11: Energy resolution for Pb + LAr geometry with merging different numbers of physical cells into 1 read-out cell.

Comparing the different merging strategies (except the "Double" the geometry itself is untouched), the resolution seems to be almost untouched by merger of cells at read-out level. However it is clearly shown again that the merger at physical level does impact the resolution for the worst. Due to the ideal detector and use of a particle gun these results are not fully reliable, however it is a good indicator that merging multiple cells at read-out level might be viable.

different merging strategies (except the Double the geometry itself is untouched)

3.4 Angular resolution

Using the clustered data, the angular resolution of the detector can also be studied. Taking a look to the ϕ resolution first, the baseline Pb + LAr geometry with different cell mergers is shown in figure 12.

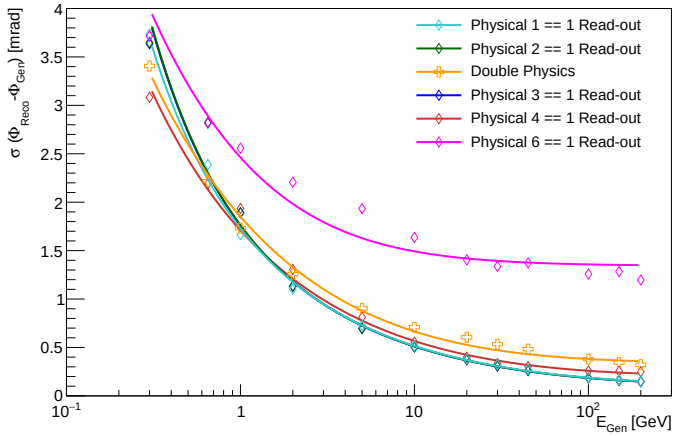

Figure 12: Phi resolution for Pb + LAr geometry with different cell mergers

Figure 12 shows a very similar resolution for a merger up to 4 cells at read-out level. The merger of two cells on physical level shows a slight degradation compared to merger at read-out level.

However, when going from a 4-1 to a 6-1 merger at read-out level, the phi resolution shows a significant degradation. Taking a deeper look into the responses fitted to obtain the ϕ resolution some non-gaussian behaviour starts to show as can be seen in figure 13.

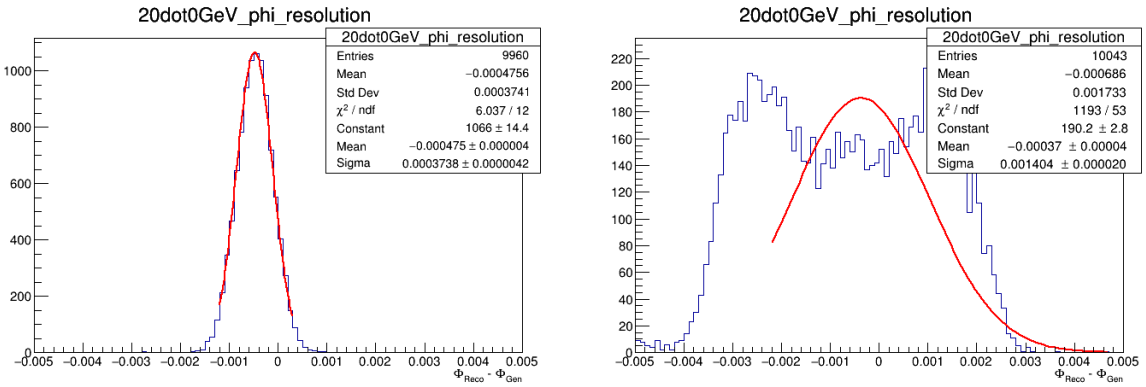

Figure 13: Detector phi response from a 4-1 merger at read-out level (left), compared to a 6-1 merger at read-out level (right)

The cause of the behaviour shown in figure 13 is as of yet still unknown and thus needs further investigation.

Moving away from the differently merged setups, the effect of the material choice on ϕ resolution is also studied. The fitted curves for different geometries are shown in figure 14.

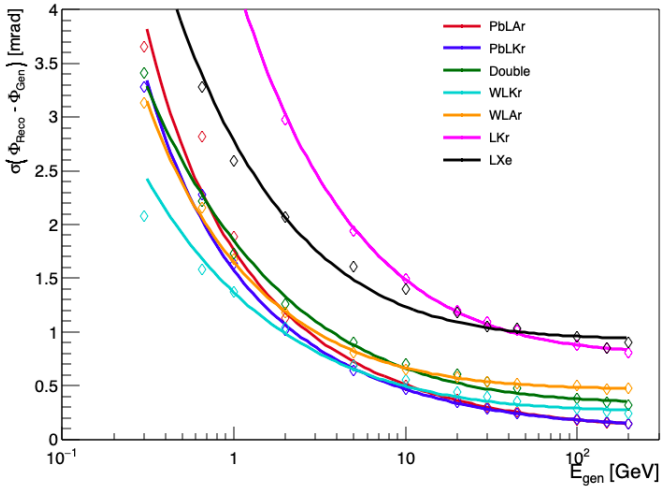

Figure 14: ϕ resolution for different geometries

Comparing the different sampling type calorimeters, a roughly similar behaviour is seen. This contrary to the homogeneous calorimeters, which show a clear step. The exact cause of the degradation has to be studied in more detail, however a plausible cause is the use of a sliding window clustering algorithm. At the moment the sliding window has a fixed size used in all performance studies and is thus not re-tuned where needed.

Part 4
Summary

In summary this report studied the impact of different geometry considerations on the detector performance of a Noble Liquid calorimeter. This is done by determining the sampling fraction and upstream/downstream corrections first. Which are in turn used for the full calorimeter reconstruction needed to study energy and angular resolution.

The dead material corrections show an improvement in detector response. While some points deviate from the fitted function, the resolution only improves.

The Pb + LKr geometry performs better than the baseline Pb + LAr geometry. However the homogeneous geometries show far superior energy resolution compared to the sampling geometries, but take up a lot of space. Geometries using W as an absorber perform worse when keeping the same absorber thickness as in the baseline. Considering halved physical cell thickness enhance the sampling frequency and makes this scenario competitive with the others.

From these studies is has been found that merging cells on a read-out level doesn't have much impact on performance up until a 4-1 merger. From a 6-1 merger on read-out level, the ϕ resolution starts to show significant degradation. When merging cells on the physical level, the energy resolution shows a degradation while keeping similar ϕ resolution.

All results shown are using a particle gun, without the inclusion of noise or detector non-uniformities, which will need to be included in future studies.

References

[1] M. Benedikt, "Future circular collider (fcc) study—status," in *Proceedings of 1st Future Hadron Collier Workshop, CERN, Geneva Switzerland*, 2014.

[2] A. Abada, M. Abbrescia, S. S. AbdusSalam, I. Abdyukhanov, J. A. Fernandez, A. Abramov, M. Aburaia, A. Acar, P. Adzic, P. Agrawal *et al.*, "Fcc physics opportunities," *The European Physical Journal C*, vol. 79, no. 6, pp. 1–161, 2019.

[3] M. Antonello, "Idea: A detector concept for future leptonic colliders," *Il nuovo cimento C*, vol. 43, no. 2-3, pp. 1–6, 2020.

[4] (2021, September). [Online]. Available: https://github.com/HEP-FCC

[5] G. Aad and et. al., "Electron and photon energy calibration with the ATLAS detector using LHC run 1 data," *The European Physical Journal C*, vol. 74, no. 10, oct 2014. [Online]. Available: https://doi.org/10.1140%2Fepjc%2Fs10052-014-3071-4

A Energy resolution fit parameters

Table 3: Fitted parameters energy resolution

Clusters	$\frac{A}{E}$	$\frac{B}{\sqrt{E}}$	C
Pb + LAr	0	0.079	0.011
Pb + LAr (double)	0	0.071	0.011
Pb + LKr	0	0.099	0.015
W + LAr	0	0.075	0.052
W + LKr	0	0.086	0.041
LKr (homo)	0	0.019	0.005
LXe (homo)	0	0.016	0.008

Cells	$\frac{A}{E}$	$\frac{B}{\sqrt{E}}$	C
Pb + LAr	0	0.077	0.021
Pb + LAr (double)	0	0.070	0.050
Pb + LKr	0	0.098	0.027
W + LAr	0	0.083	0.050
W + LKr	0	0.085	0.041
LKr (homo)	0.004	0	0.008
LXe (homo)	0	0.007	0.010

B W + LKr fit parameters

Clusters	$\frac{A}{E}$	$\frac{B}{\sqrt{E}}$	C
W + LKr (Up Corr.)	0	0.086	0.041
W + LKr (Up+Down Corr.)	0	0.096	0.026
W + LKr (halved Up Corr.)	0	0.064	0.027
W + LKr (halved Up+Down Corr.)	0	0.075	0.015

Part 5
Acknowledgements

I am very grateful to be given the great opportunity to attend the CERN summer school 2021. It was a great experience to attent the lectures as well as to be part of the FCC R&D process.

I also want to say a special thanks to my supervisors for helping me do some really interesting research. Finally I want to thank my friends for keeping me motivated and letting me relax.